Modeling the Interface Between Two Layers of Snow

H.P. Marshall[1]

Institute of Arctic and Alpine Research
Department of Civil, Environmental and Architectural Engineering
University of Colorado at Boulder, Boulder, CO 80309, U.S.A.

Abstract: Although dry slab avalanches in maritime climates can occur due to failure within a layer, avalanches in more continental climates are often caused by a weak bond between layers, usually as a result of the presence of surface and/or depth hoar. This can make modeling such a situation complex, as the quantitative material properties of the strength between two layers are difficult to measure and poorly understood. In addition, it is well known that the strength of snow shows a large degree of spatial variability. Measurements indicate local areas of the snowpack can have a strength which is less than the overburden stress, while the slope remains intact. The stress due the weight of snow above these areas is redistributed to areas of greater strength, a phenomenon which has been termed "bridging". Interface elements for use in finite element analysis have been developed in structural mechanics, which simulate the interface between two different materials (i.e. layers) and allow modeling of discontinuities within in a continuous system, as well as allowing the traditional elements within the model to slip relative to one another. Preliminary finite element modeling with these interface elements in the context of snow slope stability indicate that they may provide a useful tool for modeling the transfer of stress from weak to strong areas within the snowpack, as well as fracture propagation of dry slab avalanches.

Keywords

snow slope stability, finite element modeling, weak layers, interfaces

1. Introduction

Snow is an extremely variable substance, and like its other physical properties, the strength of snow has been a very difficult parameter to accurately model, due to its wide variation in seemingly similar situations. Snow strength depends strongly on microstructure [*Hansen and Brown*, 1987], however microstructural properties are rarely measured. Current snow strength models based on density show a wide range of scatter [*Jamieson*, 1995], [*McClung*, 1974], but remain useful for the prediction of direct action avalanches [*Conway and Wilbour*, 1999].

The majority of this large scatter in strength measurements is believed to be due to true variability in the material properties and not due to measurement error. Numerous studies have shown standard deviations of $\sim 25 - 50\%$ are common [*Fohn*, 1987], [*Sommerfeld and King*, 1979] within a seemingly homogeneous layer of snow.

Measurements along the crownwall of recent avalanche sites indicate that snow slopes consist of weak areas (deficit zones) where the shear strength is less than the overburden stress, and strong areas (pinning zones) where the shear strength is often much greater than the overburden [*Conway and Abrahamson*, 1988]. This situation is also often observed in continental climates, when the depth hoar layer is very weak, and the snowpack is supported by trees and stronger areas along the side of avalanche-prone slopes. This phenomenon has been termed "bridging", and has gained much interest although it seems to be poorly understood.

Previous approaches to modeling this problem of wide strength variation have used statistical methods [*Sommerfeld*, 1980], [*Gubler*, 1978], [*Sommerfeld*, 1971], by calculating a probability of failure. The two common statistical theories that have been proposed are the series-element theory [*Weibull*, 1939] and the parallel-element theory [*Daniels*, 1945]. For predicting shear failure of snow, it appears that Daniel's parallel-element theory provides the most accurate description, while tensile tests appear to exhibit a mixture of series- and parallel- element behavior [*Sommerfeld*, 1980]. Using a Daniels- [1945]

[1]Corresponding author address: H.P. Marshall, INSTAAR, University of Colorado at Boulder, 1560 30th St, Campus Box 450, Boulder, CO 80309, USA; tel: (303) 735-8167; email: marshalh@colorado.edu.

type correction to a large number of shear frame tests appears to provide a useful measure of the strength of a weak layer [*Sommerfeld and King*, 1979], however this type of test is so time intensive (at least 50 shear frame tests required) that it does not seem to have been adopted as common practice for snow slope stability evaluation.

This variability, however, is becoming an increasingly important problem as the number of backcountry travelers continues to rise. With snow strength showing such large variations, digging one or two snowpits to evaluate the stability of a slope may not be sufficient. Due to the nature of the "bridging" phenomenon, it seems that a model in two- and preferably three-dimensions which incorporates the observed distribution of strength and describes the transfer of load, may lead to a better understanding of the physical processes involved.

This paper presents an alternative approach to this problem, by forming the basis for finite element modeling of the bond between two layers of snow, and providing a means for mathematically representing the transfer of load from weak or deficit zones to strong or pinning zones. In order to model discontinuities in a continuous system, and allow elements to move relative to one another, an element which represents the interface between two layers is required. *Interface elements* have been developed in the structural engineering community [*Desai and Rigby*, 1995], [*Beer*, 1985] for solid/fracture mechanics problems, to simulate the transfer of load due to microcracking, and for prediction of the origin and shape of fractures in various materials, most notably concrete [*Willam and Rhee*, 2001]. Here we present preliminary tests to investigate the applicability of these elements to snow slope stability problems.

2. Finite Element Modeling

With the rapid increase in computing power in the last 20 years, the finite element method has become a widely used approach for a large variety of problems. The advantage of this technique is that it can be applied to any geometry, and effects of non-homogeneity as well as non-linear and time-dependent properties can be incorporated for situations where analytic solutions would be extremely complex or impossible to find. A short description of the technique will be given here, as it has been thoroughly described elsewhere [*Cook et al.*, 1989].

The body to be studied, which can take any desired shape, is first divided into many small elements. The elements used in this study are *constant strain triangles* (CST) and *interface elements*, for which the stresses and strains are assumed constant. The equilibrium conditions and compatibility are satisfied between elements, and these conditions along with the stress-strain law are satisfied within each element. The solution from the finite element method approaches the analytic solution as the number of elements is increased, for those problems for which such a solution is available. The solution of a set of governing equations can be found at many points throughout the domain, as the problem is formulated as a large system of algebraic equations which a computer can easily solve. The system of algebraic equations is typically written as:

$$\mathbf{F} = \underline{\mathbf{K}}\mathbf{u} \tag{1}$$

where $\mathbf{F}$ and $\mathbf{u}$ are column vectors which contain the nodal forces and displacements, respectively, and $\underline{\mathbf{K}}$ is the *stiffness matrix* which depends on the material properties of the elements, as well as their size and shape. In two dimensions, the size of $\mathbf{F}$ and $\mathbf{u}$ is $[2n \times 1]$ where n is the number of nodes and the size of $\underline{\mathbf{K}}$ is $[2n \times 2n]$. Either the force or the displacement is specified at every node on the boundary, and Eqn. 1 is solved for the unknown displacements. These unknown displacements can then be used to calculate the nodal forces, and the stresses and strains within each element.

As *interface elements* are not part of typical commercial finite element packages (such as ABAQUS, PLAXIS, etc), this model was created by modifying code written in *Mathematica* by Rhee [2002]. At this stage the results can be computed in a reasonable amount of time on an IBM ThinkPad 770z, however further detailed analysis with large numbers of elements will be run on the supercomputer at the Institute of Arctic and Alpine Research.

3. Interface Elements

Interface elements provide a method for modeling the accumulation of microstresses in the neighborhood of defects, and the breaking of bonds. They allow modeling of microcracks which coalesce to initiate the formation of mesoscale cracks. Thus, these elements provide a powerful tool for the study of fracture mechanics. The solid/fracture mechanics community has initiated interest in the study of the behavior of structures containing interfaces between two dissimilar materials, as these interfaces have a substantial influence on the response of the structure to loading. Modeling discontinuities within a continuous system requires an element with realistic constitutive properties and the ability to simulate the material interface [*Plesha and Ballarini*, 1989].

The interface element used in this paper is based on the element proposed by [*Hohberg*, 1995] and [*Beer*, 1985], used for modeling fracture in concrete. Analogous to the relationship between stress σ and

strain ε ($\sigma = E\varepsilon$), the traction τ of the cohesive surface defined by the interface element is related to the separation $\mathbf{v}$ of the cohesive surface as

$$\tau = \underline{\mathbf{D^e}}\mathbf{v} \tag{2}$$

where $\tau = [\tau_t, \tau_n]^T$ and $\mathbf{v} = [v_t, v_n]^T$ are comprised of the normal and tangential components, and $\underline{\mathbf{D^e}} = \underline{\mathbf{D^e}}(\mathbf{v})$ is a non-linear function of $\mathbf{v}$. Because this type of constitutive equation is non-linear (i.e. $\tau(\mathbf{v})$ is non-linear), and the finite element formulation is based on solving a set of linear algebraic equations, we must solve for the unknown displacements in a series of steps. In each successive step, the current tangent stiffness or rate constitutive equation for the cohesive surface is used to approximate $\underline{\mathbf{D^e}}$, as is typically done for non-linear constitutive relations. The next section outlines the calculation of the tangent stiffness matrix $\underline{\mathbf{D^t}}$.

3.1 Tangent Stiffness Matrix $\underline{\mathbf{D^t}}$

Traditionally, the isotropic damage relation is:

$$\tau = (1-\omega)\underline{\mathbf{D}}\mathbf{v} \tag{3}$$

where $\tau = [\tau_t, \tau_n]^T$ and $\mathbf{v} = [v_t, v_n]^T$ represent the normal and tangential components of the traction and separation of the cohesive surface, respectively, as above. As long as damage has not been initiated, we assume that the normal and tangential stiffnesses are equal and that there is no coupling between the normal and tangential separation. Therefore, initially, we let

$$\underline{\mathbf{D}} = d_0\underline{\mathbf{I}} = \begin{bmatrix} d_0 & 0 \\ 0 & d_0 \end{bmatrix} \tag{4}$$

where d_0 is the elastic cohesive surface stiffness and $\underline{\mathbf{I}}$ is the identity matrix. In the ideal situation one would use a micromechanically based evolution for the damage variable ω, based on current work on the micromechanics of snow [*Johnson and Schneebeli*, 1999], but here we begin by following Rhee [2002] and simply assume that ω is a function of the one-dimensional cohesive separation ζ, which is defined as

$$\zeta^2 = v_t^2 + v_n^2. \tag{5}$$

Our constitutive relationship is non-linear, as stated above, therefore we must approximate $\underline{\mathbf{D^e}}$ in a series of steps using the tangent stiffness matrix $\underline{\mathbf{D^t}}$. To obtain the rate constitutive equation for calculating the tangent stiffness matrix, we must differentiate Eqn. 3

$$\dot{\tau} = (1-\omega)\underline{\mathbf{D}}\dot{\mathbf{v}} - \dot{\omega}\underline{\mathbf{D}}\mathbf{v}. \tag{6}$$

Since $\omega(\zeta)$ is a function of ζ, we find $\dot{\omega}$ as

$$\dot{\omega} = \frac{\partial\omega}{\partial\zeta}\left[\frac{\partial\zeta}{\partial v_n}\dot{v}_n + \frac{\partial\zeta}{\partial v_t}\dot{v}_t\right] = \frac{\partial\omega}{\partial\zeta}\left[\frac{v_n}{\zeta}\dot{v}_n + \frac{v_t}{\zeta}\dot{v}_t\right] \tag{7}$$

where the last step comes directly from differentiating Eqn. 5. Substituting Eqn. 7 into Eqn. 6 and rearranging terms we arrive at the rate constitutive equation

$$\begin{bmatrix} \dot{\tau}_t \\ \dot{\tau}_n \end{bmatrix} = \underline{\mathbf{D^t}} \begin{bmatrix} \dot{v}_t \\ \dot{v}_n \end{bmatrix} \tag{8}$$

where

$$\underline{\mathbf{D^t}} = (1-\omega)\underline{\mathbf{D}} - \underline{\mathbf{D_2}} \tag{9}$$

and $\underline{\mathbf{D_2}} =$

$$\begin{bmatrix} -\frac{\partial\omega}{\partial\zeta}\frac{v_t}{\zeta}d_0v_t & -\frac{\partial\omega}{\partial\zeta}\frac{v_n}{\zeta}d_0v_t \\ -\frac{\partial\omega}{\partial\zeta}\frac{v_t}{\zeta}d_0v_n & -\frac{\partial\omega}{\partial\zeta}\frac{v_n}{\zeta}d_0v_n \end{bmatrix} \tag{10}$$

In order to calculate ω and $\frac{\partial\omega}{\partial\zeta}$, we find the one-dimensional traction of the cohesive surface $\sigma(\zeta)$ using Eqn. 3 and Eqn. 5, and solve this for ω

$$\sigma(\zeta) = (1-\omega(\zeta))d_0\zeta \tag{11}$$

$$\omega(\zeta) = 1 - \frac{\sigma(\zeta)}{d_0\zeta} \tag{12}$$

therefore

$$\frac{\partial\omega}{\partial\zeta} = \frac{1}{d_0\zeta}\left(\frac{\sigma(\zeta)}{\zeta} - \frac{\partial\sigma(\zeta)}{\partial\zeta}\right). \tag{13}$$

The last step we must take is to define the one-dimensional traction of the cohesive surface $\sigma(\zeta)$. Initially we assume that the interface exhibits linear elastic behavior, and let $\sigma(\zeta) = d_0\zeta$, where $d_0 = \sigma_{max}/\delta_{max}$, σ_{max} is the shear strength of the cohesive surface, and δ_{max} is the one-dimensional separation ζ at which damage is initiated. For $\zeta < \delta_{max}$, we find $\frac{\partial\sigma}{\partial\zeta} = \sigma_{max}/\delta_{max}$. Commonly a softening response is assumed after damage is initiated, which is either linear or exponential. Here we assume a softening response which is exponential, and for $\zeta > \delta_{max}$ we define

$$\sigma(\zeta) = \sigma_{max}\, e^{(\delta_{max}-\zeta)/(\delta_r-\delta_{max})} \tag{14}$$

where δ_r determines the rate of softening. Therefore, for $\zeta > \delta_{max}$ we have

$$\frac{\partial\sigma}{\partial\zeta} = -\frac{1}{\delta_r - \delta_{max}}\,\sigma_{max}\, e^{(\delta_{max}-\zeta)/(\delta_r-\delta_{max})}. \tag{15}$$

Using the above equations, the tangent stiffness matrix $\underline{\mathbf{D^t}}$ can be calculated during each successive iteration, which allows the finite element solution to this non-linear problem.

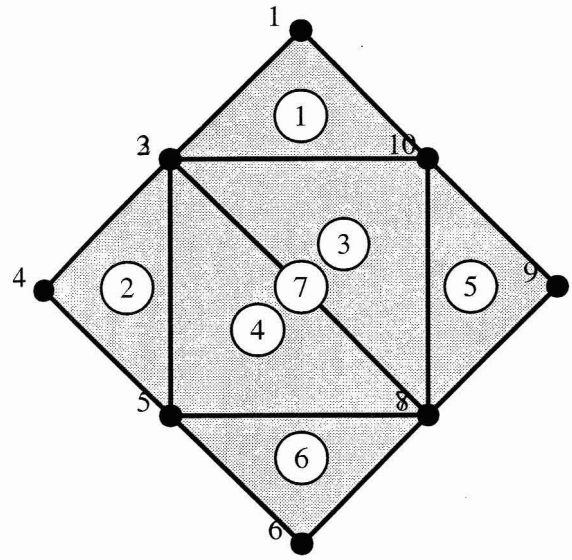

Figure 1. *Basic building block for finite element analysis, containing 6 constant strain triangles and one interface element. Note that nodes 2,3 and 7,8 have the same coordinates, as the interface element (7) has zero thickness. The x-axis is parallel to the slope and positive in the downslope direction; the y-axis is perpendicular to the slope and positive upwards.*

4. Basic Building Block

In this paper we restrict the interface elements to exist only on a plane parallel to the slope, as initially we are just investigating the applicability of the model to shear failure. We begin with the basic building block for our finite element analysis, which consists of 6 *constant strain triangles* and one *interface element*, shown in Fig. 1.

Our coordinate system is defined with the x-axis parallel to the slope and positive in the downslope direction; the y-axis is perpendicular to the slope and positive upwards. Element labels are shown within circles, and nodes are numbered. Element 7 is the interface element, which has zero thickness, and therefore initially nodes 2,3 and 7,8 have the same coordinates.

Following previous finite element modeling of snow slopes [*Wilson et al.*, 1999], [*Curtis and Smith*, 1974], [*Smith*, 1972], [*Smith et al.*, 1971] we assume that each layer is linearly elastic and plane strain conditions accurately describe a snow slope. Snow surely represents non-linear behavior, however deformation within the snowpack due to the weight of a skier causes a strain-rate $\dot{\varepsilon} > 10^{-4}$, therefore the linear assumption should be appropriate for many situations [*Wilson et al.*, 1999]. As in previous modeling work, we begin with the two-dimensional assumption of plane strain as gradients across the slope are most likely smaller [*Fohn*, 1987], however future work will extend this model to three-dimensions to more completely describe the "bridging" effect.

In this first simple initial study the elastic modulus E and Poisson's ratio ν are assumed to be constant, however this assumption will be relaxed later as well. This model was initially developed as a *displacement-based* formulation, such that prescribed displacements are applied incrementally (due to the non-linear nature of the interface elements), and the required forces to sustain those displacements as well as the resulting stresses and strains are calculated after the solution of the unknown degrees of freedom is found. To test this basic building block, we apply a vertical deformation incrementally at node 1, to attempt to initiate shear failure of the block. The nodes along the bottom of the block are assumed fixed, as initially we assume that the snowpack is fixed to the ground (i.e. no full-depth / climax avalanches will occur).

4.1 Results

This first test produced satisfactory results, as shear failure was initiated and the upper three constant strain triangles sliped together relative to the lower three CST. The deformed configuration is shown in Fig. 2.

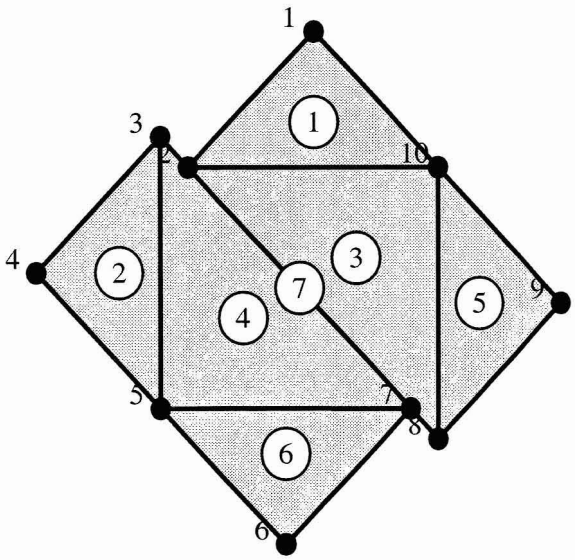

Figure 2. *Deformed configuration of basic building block, after incremental vertical displacement was applied at node 1. Upper three CST slip relative to lower three CST, as the interface element allows modeling of shear failure.*

Note that the upper three CST do deform slightly, however the majority of displacement is due to the

failure of the interface element. Changing the material properties of the interface element and the constant strain triangles can be easily done to represent a stronger or weaker bond of the two layers relative to the stiffness of the layers themselves, resulting in a wide range of possible behavior.

Fig. 3 shows the tangential displacement u_x at node 1 vs. the resulting tangential force f_x at node 1. Note that there are three regions of behavior, labeled **A,B,C** in the figure.

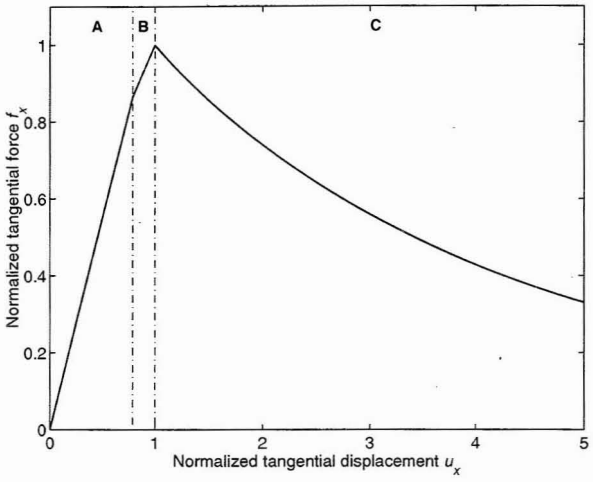

Figure 3. *Tangential displacement u_x vs. resulting tangential force f_x at node 1. The three regions of behavior are labeled* **A,B,C**. *The force rises to a peak, then after damage is initiated within the interface element, there is an exponential decay to near zero force.*

Region **A** represents the elastic deformation of the upper three constant strain triangles. Region **B** represents deformation of both the constant strain triangles as well as initial deformation of the interface element. Before damage is initiated, the interface element exhibits linear elastic behavior, as described in the preceding section. Region **C** begins when damage occurs in the interface element, and the exponential decay is caused by the softening response.

This initial simple example demonstrates the basic characteristics of the interface element. For a incremental applied displacement, the required force rises linearly with increased displacement as the upper elements deform. The slope of this line changes as the interface element begins to deform as well, and there is an exponential decay to zero of the required force as damage is initiated and the upper three constant strain triangles slip relative to the lower three. This basic building block will be used to describe progressive shear failure between two layers of snow.

5. 18 Constant Strain Triangles and 3 Interface Elements

Next we extend this concept to multiple interface elements, to examine the behavior as each element fails in succession and load is transferred. We begin by combining three of the basic building blocks outlined in the previous section. This amounts to 18 constant strain triangles, and 3 interface elements. As before, the interface elements initially have zero thickness, therefore there are several nodes with the same coordinates. The initial configuration is shown in Fig. 4.

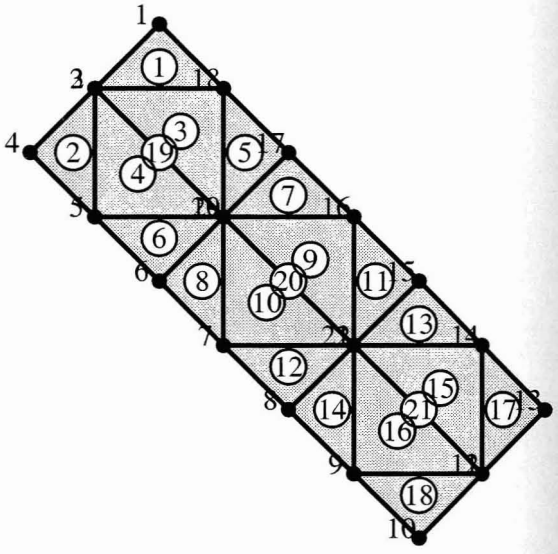

Figure 4. *Initial configuration of the combination of three building blocks. The coordinate system is the same as that in Fig. 1, and incremental vertical displacement was applied at node 1 as before.*

Once again, we apply an incremental vertical displacement at node 1, and evaluate the resulting forces, stresses, and strains at each node and element during each step. As before, shear failure was initiated, as the upper constant strain triangles eventually slipped relative to the lower CST, due to the failure of the interface elements. However, since there are now three separate interface elements, the process of failure is more complicated.

5.1 Tangential Force vs Displacement

First we examine the required tangential force at node 1 vs. to the incremental tangential displacement. This is shown in Fig. 5. We now have five different regions of behavior, as the interface elements do not deform and fail at the same time. These five regions are labeled **A,B,C,D,E**.

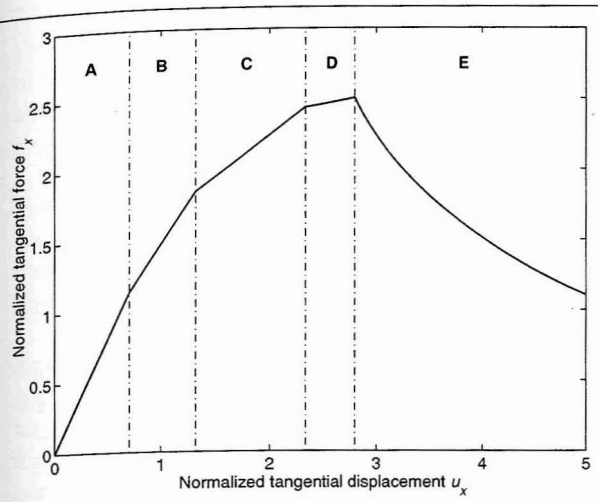

Figure 5. *Tangential displacement u_x vs. resulting tangential force f_x at node 1. The five regions of behavior are labeled* **A,B,C,D,E**. *The force rises to a peak, but the slope changes as each interface element successively begins to deform. After damage is initiated within all three interface elements, there is an exponential decay to near zero force.*

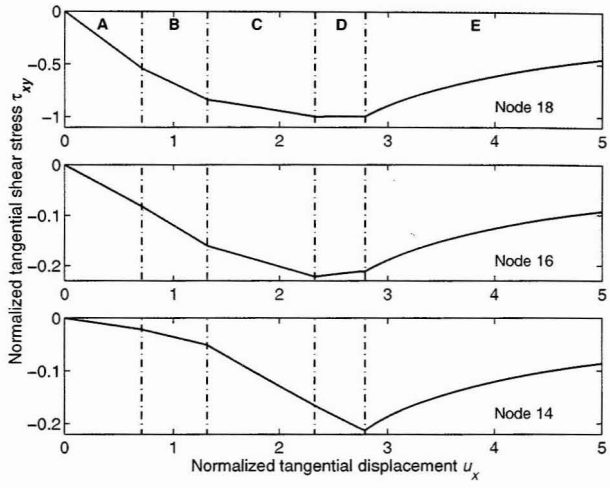

Figure 6. *Tangential displacement u_x vs. tangential shear stress τ_{xy} at node 1. The five regions of behavior are labeled* **A,B,C,D,E**. *The shear stress is negative, as expected for the given coordinate system. As each interface element progressively deforms, the load is transferred to the downslope element until all three have failed, at which point all nodes show an exponential decay to near zero.*

Region **A** shows the initial deformation of the upper constant strain triangles, as before. Region **B** indicates initial deformation of the first interface element (element 19), along with continued deformation of the upper CST. Regions **C** and **D** show deformation with contributions from the second and third interface elements (elements 20, 21), respectively. The slope continues to decrease, as more and more elements are involved in the deformation. Region **E** begins when damage has initiated in all three interface elements, as the tangential force then decays exponentially to near zero.

Note that the exponential decay of the tangential force does not begin until all three interface elements have failed. As each successive interface element deforms, the stress which it was bearing is transferred to the downslope elements, representing the "bridging" phenomenon discussed earlier.

5.2 Shear Stress vs Displacement

In this section we investigate the shear stress at three different points along the slope as a function of the applied displacement. Fig. 6 shows the slope parallel shear stress τ_{xy} for nodes 18, 16, and 14 as a function of the incremental displacement at node 1. Regions **A,B,C,D,E** identical to those in Fig. 5 are shown for reference. These nodes were chosen as each is located in the center of one of the three interface elements.

In region **A**, none of the interface elements have begun to deform, and all three nodes show a linearly increasing shear stress. The shear stresses are all negative, as expected for our coordinate system and the direction of deformation. In region **B**, the first interface element begins to deform (element 19), which causes a decrease in the slope of shear stress at node 18. This is because each increment of displacement causes less stress at node 18 due to the deformation of the interface element. Note that the slope of the shear stress curve at nodes 16 and 14 increase slightly as some of the load is transferred to the two downslope building blocks.

In region **C** the second interface element (element 20) begins to deform, causing a decrease in the slope of the shear stress curve at nodes 18 and 16, and an increase in slope at node 14. This is expected, as more deformation now occurs in the third building block due to the transfer of load from the upper two building blocks.

Region **D** shows the slope of the shear stress curve decreasing again at nodes 18 and 16, however there is little change in slope at node 14. One would expect the slope at node 14 to decrease as well, however there are no downslope blocks left to transfer the load to. This effect is due to the small number of elements in this simple example. Finally, in region **E** all three interface elements have failed, and all three nodes show an exponential decline to near zero.

This simple example problem shows successive transfer of load as each interface begins to deform in turn. The upper layer does not fail, however, until all three interfaces have each failed. This indicates that these interface elements may provide a tool for describing the transfer of load from deficit zones to pining zones. The next section will make

the changes in each region more apparent by looking at the derivative $\partial\tau_{xy}/\partial u_x$.

5.3 Change in Shear Stress vs Displacement

As the changes in slope of the shear stress curves are not completely obvious in Fig. 6, next we plot the slope of these curves $\partial\tau_{xy}/\partial u_x$ vs. the applied tangential displacement u_x. These are shown again for nodes 18, 16, and 14 in Fig. 7, with the five regions of behavior once again labeled.

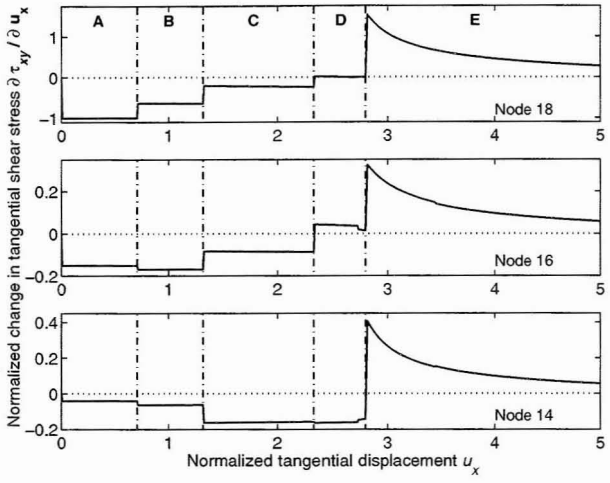

Figure 7. *Tangential displacement u_x vs. change in tangential shear stress $\partial\tau_{xy}/\partial u_x$ at node 1. The five regions of behavior are labeled* **A,B,C,D,E**. *The change in shear stress shows the transfer of load between building blocks until all three interface elements have failed, at which point the slope rapidly becomes positive and then decays exponentially to zero.*

In region **A** as the upper CST begin to deform, all three nodes have a (negative) increase in shear stress as expected from the coordinate system definition. In region **B**, as the first interface element (element 19) begins to deform, the node above that element (node 18) shows a decrease in slope as load is transferred to the downslope building blocks. In region **C** the second interface element (element 20) has begun to deform, causing node 18 and 16 to show a decrease in $\partial\tau_{xy}/\partial u_x$ as much of the load is now transferred to the lowest building block.

Region **D** shows the third interface element (element 21) start to deform, which causes the slope of shear stress to decrease at nodes 18 and 16, and should cause a decrease in shear stress slope at node 14. However, there are no downslope building blocks left to transfer the load to, and since we have left the right-hand edge of our configuration free and not fixed, this third block must continue to support the load.

Finally, in region **E**, damage has been initiated in all three interface elements, and the slope of the shear stress curve at all three nodes rises rapidly to a positive value (so that the negative shear stresses decrease), then exponentially decays to near zero, as the upper layer slides relative to the lower layer. Fig. 7 clearly shows the transfer of load as each interface element becomes involved in the deformation, and indicates that all three interface elements must fail before failure is initiated in the upper layer.

6. Future Work

These simple initial tests have allowed a thorough understanding of the behavior of interface elements in shear failure, and indicate that they may provide a useful tool for modeling snow slope failure. More complicated tests will now be performed, with a realistic slope geometry and many elements. The supercomputer at the Institute of Arctic and Alpine Research (INSTAAR) will provide enough computing power for the solution of much more complicated problems.

Another planned improvement for the model will be to include nodal forces as boundary conditions. Currently the finite element model is of the *displacement-based* type, where displacements are (incrementally, for non-linear problems) prescribed, and forces are calculated after the solution of the unknown displacements is found. The method of solution will be made more robust so that forces as well as displacements can be applied to any of the nodes as initial conditions. This will allow one to include the force of gravity everywhere throughout the snowpack, as well as apply the force of a skier, climber, or snowmobile, making the model more physically realistic.

Further planned improvements include modeling of layers with different properties, and the inclusion of statistical distributions of interface layer strengths. Eventually, vertical interface elements will be included as well, to attempt to predict the location and shape of fracture profiles. Finally, extending this model to three-dimensions will allow a more complete mathematical description of stress redistribution ("bridging") within a winter snowpack.

7. Conclusions

This preliminary work with interface elements in a finite element model has shown that these types of elements may provide a tool for modeling the bond between two layers of snow on an avalanche-prone slope. These simple tests provide an initial understanding of the behavior of interface elements, and lay the groundwork for future modeling efforts of this type. Shear failure can be modeled with this method, which allows more traditional elements to

slip relative to one another. By varying the strength of individual interface elements, this method may be able to more accurately describe the strength properties of a snow slope. In addition, they provide a means to accurately model the transfer of stress or load from weak areas (deficit zones) to strong areas (pinning zones). This may lead to greater insight about physical processes of this "bridging" phenomenon.

If a method for accurately estimating the shear strength of a snow slope over a large area is found (possibly ground penetrating radar), this type of modeling would allow one to incorporate this information into a slope-specific model. Previous work has clearly shown that all snow properties, in particular snow strength, vary widely across a snow slope. Hopefully this type of model will provide a means for mathematically describing this variation and its affect on the distribution of stress. Further work with interface elements could lead to the prediction of the location and shape of fracture profiles.

Acknowledgments

This research was funded by an Earth Systems Science NASA Graduate Research Fellowship. The author is indebted to Inkyu Rhee who provided access to his original code and comprehensive exam [*Rhee*, 2002], which was written to simulate tensile fracture in concrete, upon which the ideas and code for this paper were built. Kaspar Willam provided several useful discussions.

References

Beer, G., An isoparametric joint/interface element for finite element analysis, *Int. Journal for Numerical Methods in Engineering*, *21*, 585–600, 1985.

Conway, H., and J. A. Abrahamson, Snowslope stability - a probabilistic approach, *Journal of Glaciology*, *34*(117), 170–177, 1988.

Conway, H., and C. Wilbour, Evolution of snow slope stability during storms, *Cold Regions Science and Technology*, *30*, 1999.

Cook, R., D. Malkus, and M. Plesha, *Concepts and applications of finite element analysis*, John Wiley and Sons, New York, 1989, 630 pp.

Curtis, J., and F. Smith, Material property and boundary condition effects on stresses in avalanche snowpacks, *Journal of Glaciology*, *13*(67), 99–108, 1974.

Daniels, H., The statistical theory of the strength of bundles of threads, *Proc. of the Royal Society of London, Ser. A*, *183*(995), 405–435, 1945.

Desai, C. S., and D. B. Rigby, Modeling and testing of interfaces, *Mechanics of Geomaterial Interfaces*, pp. 107–125, 1995.

Fohn, P. M. B., The stability index and various triggering mechanisms, in *Avalanche Movement and Effects. Proc., Davos Symposium*, no. 162, pp. 195–214, Int. Ass. Hydrol. Sci., 1987.

Gubler, H., An alternate statistical interpretation of the strength of snow, *Journal of Glaciology*, *20*(83), 343–357, 1978.

Hansen, A. C., and R. L. Brown, A new constitutive theory for snow based on a micro-mechanical approach, in *Avalanche Movement and Effects. Proc. Davos Symposium*, no. 162, pp. 87–104, Int. Ass. Hydrol. Sci., 1987.

Hohberg, J. M., Concrete joints, *Mechanics of Geomaterial Interfaces*, pp. 421–445, 1995.

Jamieson, J. B., Avalanche prediction for persistent snow slabs, Ph.D. thesis, Dept. Civil Eng., Univ. Calgary, Alberta, Canada, 1995, 258pp.

Johnson, J. B., and M. Schneebeli, Characterizing the microstructural and micromechanical properties of snow, *Cold Regions Science and Technology*, *30*, 91–100, 1999.

McClung, D. M., Avalanche defense mechanisms, Ph.D. thesis, University of Washington, Seattle, Washington, 1974, 103pp.

Plesha, M., and R. Ballarini, Constitutive model and finite element procedure for dilatant contact problems, *Journal of Engineering Mechanics*, *115*(12), 2649–2668, 1989.

Rhee, I., Interface model of cohesive damage at finite element and structure levels (unpublished comprehensive exam), Ph.D. thesis, Dept. Civil, Envir. and Arch. Eng., Univ. Colorado at Boulder, Boulder, CO, USA, 2002, 71pp.

Smith, F., Elastic stresses in layered snow packs, *Journal of Glaciology*, *11*(63), 407–414, 1972.

Smith, F., R. Sommerfeld, and R. Bailey, Finite-element stress analysis of avalanche snowpacks, *Journal of Glaciology*, *10*(60), 401–405, 1971.

Sommerfeld, R., The relationship between density and tensile strength in snow, *Journal of Glaciology*, *10*(60), 357–362, 1971.

Sommerfeld, R., Statistical models of snow strength, *Journal of Glaciology*, *26*(94), 217–223, 1980.

Sommerfeld, R., and R. M. King, A recommendation for the application of the Roch index for slab avalanche release, *Journal of Glaciology*, *22*(88), 547–549, 1979.

Weibull, W., A statistical theory of the strength of materials, *Ingeniorsvetenskapsakademiens Handlingar*, (151), 1939.

Willam, K., and I. Rhee, Deterioration analysis of materials and structures, *Engineering Computations*, *18*(3/4), 690–718, 2001.

Wilson, A., J. Schweizer, C. D. Johnston, and J. B. Jamieson, Effects of surface warming of a dry snowpack, *Cold Regions Science and Technology*, *30*, 59–65, 1999.

Corresponding author address: H. P. Marshall, Institute of Arctic and Alpine Research, University of Colorado at Boulder, Department of Civil, Environmental, and Architectural Engineering, 1560 30th St, Campus Box 450, Boulder, CO 80309, USA; tel: (303) 735-8167; email: marshalh@colorado.edu.

This preprint was prepared with AGU's LaTeX macros v4, with the extension package 'AGU^{++}' by P. W. Daly, version 1.5d from 1997/04/28.